*Electronic Supplementary Information (ESI)*

# A luminescent supramolecular adduct $Cu_2I_2(NH_3)_2$-sandwiched $Cu_3(pyrazolate)_3$ as a temperature sensor

Shun-Ze Zhan,[*a] Xia Jiang,[a] Ji Zheng,[b] Xin-Da Huang,[a] Guang-Hui Chen[a] and Dan Li[*b]

[a] Department of Chemistry and Key Laboratory for Preparation and Application of Ordered Structural Materials of Guangdong Province, Shantou University, Shantou 515063, P. R. China

[b] College of Chemistry and Materials Science, Jinan University, Guangzhou 510632, P. R. China

*E-mail:* szzhan@stu.edu.cn; danli@jnu.edu.cn

# Table of Contents

## Section 1: Experimental Section

**Materials and Physical Measurements**

Commercially available chemicals were purchased and used without further purification. Infrared spectrum (IR) was obtained in KBr disk on a Nicolet Avatar 360 FTIR spectrometer in the range of 4000–400 cm$^{-1}$; abbreviations used for the IR bands are: w = weak, m = medium, b = broad, s = strong, vs = very strong. Elemental analysis (EA) of C, H, N and S was determined with an Elementar Vario EL III CHNS analyzer. Thermogravimetric analysis (TGA) was performed on a TA Instruments Q50 Thermogravimetric Analyzer under a nitrogen flow of 40 mL·min$^{-1}$ at a heating rate of 10 °C·min$^{-1}$. Powder X-ray diffraction (PXRD) experiment was performed on a D8 Advance X-ray diffractometer. $^{1}$H NMR spectroscopy was performed on a Bruker DPX 400 spectrometer using Si(CH$_3$)$_4$ (TMS) as the internal standard, and all δ values are given in ppm.

The diffuse reflectance solid-state UV-Vis spectrum was recorded on a Lambda950 UV/Vis/NIR spectrophotometer of Perkin Elmer using pure powder sample. Steady-state photoluminescence spectra and lifetime were measured with an Edinburgh FLS920 single photon counting spectrometer equipped with a continuous Xe900 xenon lamp, a μF900 μs flash lamp, a red-sensitive Peltier-cooled Hamamatsu R928P photomultiplier tube (PMT), and a closed–cycle cryostat using liquid helium as cooling medium (Advanced Research Systems). The corrections of excitation and emission for the detector response were performed ranging from 200 to 900 nm. The data were analyzed by iterative convolution of the luminescence decay profile with the instrument response function using the software package provided by Edinburgh Instruments. Lifetime data were fitted with biexponential decay functions. The goodness of the nonlinear least-squares fit was judged by the reduced $\chi^2$ value (< 1.5 in most cases). PL QY values was collected by an absolute PL quantum yield spectrometer, Quantaurus-QY C11347-11 (Hamamatsu Photovics K. K., Japan) using a Xenon light source (150 W). In all cases, the crystalline sample was selected under a microscope with 40-time amplification after being washed with ethanol then dried.

The phase purity of the sample is assured by elemental analysis and PXRD measurement (Fig. S2).

**Synthesis**

**Ligand:** The ligand 4-(1-methyl-tetrazol-5-ylthio)-3,5-dimethyl-1*H*-pyrazole (HL) was synthesized according to the literatures [S1] with modification.

5-Mercapto-1-methyltetrazole (2.32 g, 20.0 mmol) was dissolved in methanol (100 mL), then 1.8 mL (about 21.6 mmol) pyridine was added. The solution was stirred at ambient temperature while 3-chloro-2,4-pentanedione (2.68 g, 20.0 mmol) in methanol (10 mL) was slowly added. The mixture was stirred for 25 h, then solvent was evaporated under reduced pressure on the rotary evaporator. The obtained solid product was washed three times with water (20 mL), and was dried on vacuum to give white intermediate product 3-(1-methyl-tetrazol-5-ylthio)-pentane-2,4-dione. Yield, 3.51 g (82%).

3-(1-methyl-tetrazol-5-ylthio)-pentane-2,4-dione (2.14 g, 10.0 mmol) was added in 80 mL ethanol and the mixture was heated until the solid was dissolved completely. Hydrazine hydrate (80%, 2.50 mL) was added with stirring. The mixture was refluxed for 10 h and then cooled and filtered to remove a small amount of white precipitate. The solvent was removed under reduced pressure on the rotary evaporator to give white solid product. The solid was washed three times with water (20 mL), then dissolved in 50 mL hot ethanol for recrystallization. Several days later, colorless single crystal was obtained to give pure ligand *H***L** as crystalline. Yield, 1.60 g (76%). IR data (KBr pellet, cm$^{-1}$): 3415 s, 3204 s, 3122 s, 2974 s, 1620 w, 1590 m, 1492 s, 1400 s, 1295 s, 1020 s, 888 m, 775 m, 710 s, 571 m. $^{1}$H NMR (400 MHz, CDCl$_3$, 300K): 2.46 (s, 2CH$_3$, 6H), 4.06 (s, CH$_3$, 3H).

**Complex** [Cu$_3$L$_3$][Cu$_2$I$_2$(NH$_3$)$_2$][Cu$_3$L$_3$] (C$_{42}$H$_{60}$Cu$_8$I$_2$N$_{38}$S$_6$): A mixture of *H***L** (6.3 mg, 0.03 mmol), CuI (11.4 mg, 0.06 mmol), cyclohexane (1.5 mL), benzene (0.5 mL), *i*-propanol (0.5 mL) and NH$_3$·H$_2$O (25% water solution, 0.2 mL) was sealed in a 6 mL Pyrex tube, heated in an oven at 140 °C for 72 h, and then slowly cooled to room temperature at a rate of −3 °C·h$^{-1}$. Colorless block crystals were obtained (15 % yield based on ligand). Anal. Calcd. for C$_{42}$H$_{60}$Cu$_8$I$_2$N$_{38}$S$_6$: C, 27.18; H, 3.26; N, 18.12; S, 10.37 %. Found: C, 27.00; H, 3.49; N, 18.01; S, 10.11 %. IR data (KBr

pellet, cm$^{-1}$): 3420 vs, 3255 s, 2905 w, 1620 m, 1572 m, 1506 s, 1410 s, 1275 m, 722 s, 571 s.

## Section 2: Crystal Data and Additional Structural Description

**Crystal Structure Determination**

Single crystal X-ray data collection for the ligand and complex at 293 K was performed on an Oxford Diffraction Gemini E (Enhance Mo X-Ray source, Kα, λ = 0.71073 Å) equipped with a graphite monochromator and ATLAS CCD detector (CrysAlis CCD, Oxford Diffraction Ltd). The data were processed using CrysAlis RED, Oxford Diffraction Ltd (CrysAlisPro 1.171.36.28, release 01-02-2013 CrysAlis171.NET).

Single crystal X-ray data collection for the complex at 100 K was performed on a Rigaku OD (Enhance Cu X-ray Source, Kα, λ = 1.54184 Å) with CCD Plate (XtaLAB Pro: Kappa single) equipped with a Rigaku low temperature N$_2$ gas spray cooler. Data were processed with the CrysAlisPro 1.171.39.7e (Rigaku Oxford Diffraction, 2015).

Structures were solved by direct methods (SHELXTL-97) and refined on $F^2$ using full-matrix last-squares (SHELXTL-97) [S2]. All non-hydrogen atoms were refined with anisotropic thermal parameters, and all hydrogen atoms were included in calculated positions and refined with isotropic thermal parameters riding on those of the parent atoms. Crystal data and structure refinements for the ligand and complex are summarized in Table S1 in the Supporting Information. Selected bond lengths and angles are given in Tables S2-S3 in the Supporting Information. CCDC nos. 1556796-1556798 contain the supplementary crystallographic data for this paper.

## Crystal Data

**Table S1** Crystal data and structure refinements for the ligand and complex.

| Parameter | *H*L | Complex (293 K) | Complex (100 K) |
|---|---|---|---|
| Chemical formula | $C_7H_{10}N_6S$ | $C_{42}H_{60}Cu_8I_2N_{38}S_6$ | $C_{42}H_{60}Cu_8I_2N_{38}S_6$ |
| Formula weight | 210.27 | 2051.76 | 2051.76 |
| Crystal system | Monoclinic | Triclinic | Triclinic |
| Space group | $P2_1/c$ | $P$-1 | $P$-1 |
| Temperature (K) | 293 | 293 | 100 |
| $a$ (Å) | 8.9716(4) | 10.4769(4) | 10.33551(13) |
| $b$ (Å) | 6.9908(4) | 11.0875(4) | 10.98757(11) |
| $c$ (Å) | 16.3989(6) | 15.7405(6) | 15.67208(18) |
| $\alpha$ (deg) | 90 | 93.946(3) | 93.96941(9) |
| $\beta$ (deg) | 97.259(4) | 95.294(3) | 95.8876(10) |
| $\gamma$ (deg) | 90 | 91.410(3) | 90.6089(9) |
| $V$ (Å$^3$) | 1020.27(8) | 1815.46(12) | 1766.42(3) |
| Z | 4 | 1 | 1 |
| $D_{Calcd}$ (g·cm$^{-3}$) | 1.369 | 1.877 | 1.929 |
| $\mu$ (mm$^{-1}$) | 0.289 | 3.380 | 11.626 |
| Reflections collected | 4575 | 11217 | 18706 |
| Unique reflections | 1797 | 6349 | 6928 |
| $R_{int}$ | 0.0234 | 0.0298 | 0.0237 |
| Goodness-of-fit on F$^2$ | 1.087 | 1.033 | 1.420 |
| $R_1$ [a] [I > 2σ(I)] | 0.0432 | 0.0492 | 0.0441 |
| $wR_2$ [b] [I > 2σ(I)] | 0.1359 | 0.1252 | 0.1517 |
| $R_1$ [a] [all refl.] | 0.0549 | 0.0699 | 0.0443 |
| $wR_2$ [b] [all refl.] | 0.1502 | 0.1419 | 0.1520 |

[a] $R_1 = \sum(||F_o| - |F_c||)/\sum|F_o|$.   [b] $wR2 = [\sum w(F_o^2 - F_c^2)^2/\sum w(F_o^2)^2]^{1/2}$.

**Table S2** Selected bond lengths and angles in the complex.

| Parameter | 293 K | 100 K |
|---|---|---|
| Bond lengths | | |
| Cu(1)-N(1) | 1.874(5) | 1.877(3) |
| Cu(2)-N(2) | 1.866(5) | 1.880(3) |
| Cu(2)-N(7) | 1.880(5) | 1.879(3) |
| Cu(3)-N(8) | 1.871(5) | 1.874(3) |
| Cu(3)-N(13) | 1.874(5) | 1.872(3) |
| Cu(1)-N(14) | 1.872(5) | 1.879(3) |
| Cu(4)-N(19) | 1.933(5) | 1.949(3) |
| Cu(4)-I(1) | 2.5339(14) | 2.5298(8) |
| Cu(4)-I(1) #1 | 2.5768(13) | 2.5899(9) |
| Bond angles | | |
| N(1)-Cu(1)-N(14) | 168.3(2) | 168.10(14) |
| N(2)-Cu(2)-N(7) | 168.3(2) | 167.92(14) |
| N(8)-Cu(3)-N(13) | 172.3(2) | 172.96(14) |
| N(19)-Cu(4)-I(1) | 120.06(18) | 121.18(11) |
| N(19)-Cu(4)-I(1)#1 | 115.49(18) | 113.59(11) |
| I(1)-Cu(4)-I(1)#1 | 124.45(5) | 125.17(3) |
| Weak interactions | | |
| Cu(1)-I(1) | 3.4760(1) | 3.4312(3) |
| Cu(2)-I(1) | 3.1972(1) | 3.1504(3) |
| Cu(3)-I(1) | 3.3034(1) | 3.3072(3) |
| Cu(1)-Cu(4) | 3.0848(1) | 3.0229(3) |
| Cu(1)-Cu(4)#1 | 3.1653(1) | 3.1121(3) |
| Cu(1)-S(3)#2 | 3.5840(1) | 3.5391(3) |
| Cu(2)-S(3)#2 | 3.7748(1) | 3.7457(3) |
| Cu(3)-S(3)#2 | 3.9434(1) | 3.8699(4) |
| Symmetry code: #1 -x, -y+1, -z; #2 -x, -y, -z | | |

**Table S3** Selected hydrogen bond lengths (Å) and angles (°) in the complex measured at 293 K.

| D-H···A | Distances | | Angles |
|---|---|---|---|
| | H···A | D···A | |
| N19-H19f···N18 | 2.20799(7) | 3.0645(1) | 161.6 |
| N19-H19e···N6A | 2.57743(8) | 3.0531(1) | 114.3 |
| N19-H19d···N6A | 2.75084(9) | 3.0531(1) | 101.3 |
| C15-H15c···N5A | 2.74020(1) | 3.6621(1) | 161.2 |
| C5A-H5aA···N17 | 3.1040(1) | 3.9852(1) | 153.3 |
| Symmetry code: A -x, -y+1, -z; | | | |

**Additional Structural Description**



(a)  (b)
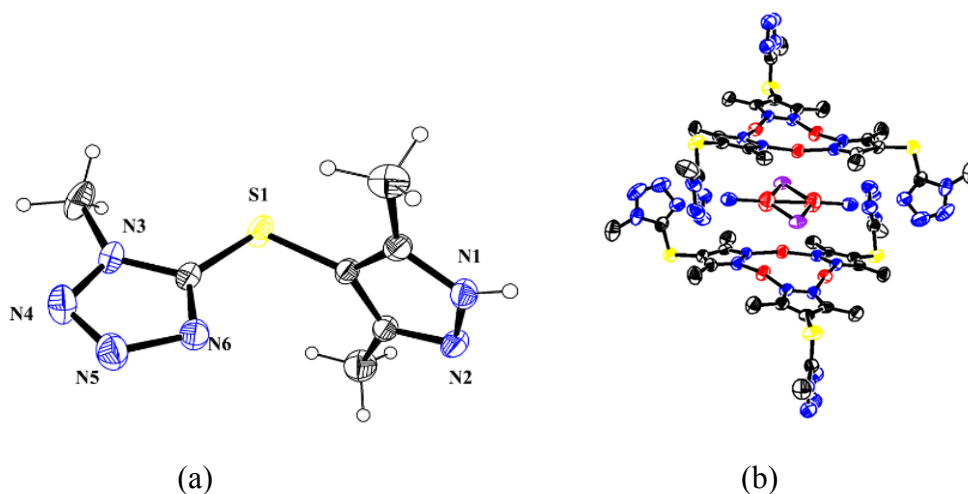
**Fig. S1** The perspective views of $H$**L** molecule (a) and the ternary adduct [Cu$_3$L$_3$][Cu$_2$I$_2$(NH$_3$)$_2$][Cu$_3$L$_3$] (b, H atoms are omitted for clarity) with 50% thermal ellipsoid. Color codes: red, Cu; blue, N; black, C; yellow, S; purple, I; white cycle, H.
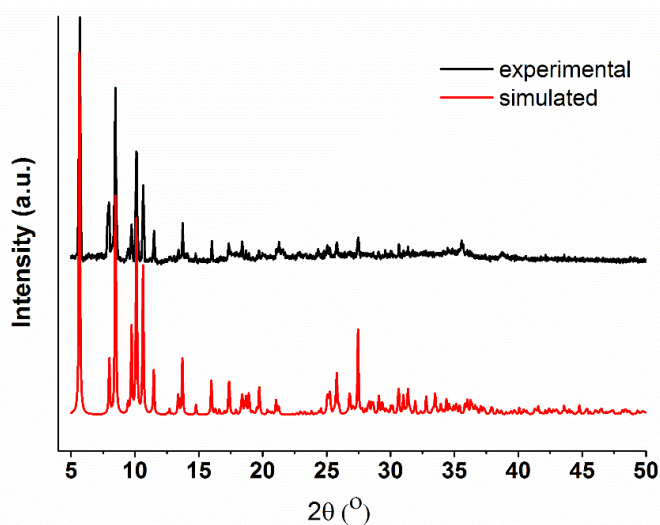


**Fig. S2** Comparison of the simulated and experimental X-ray powder diffraction patterns of the complex.
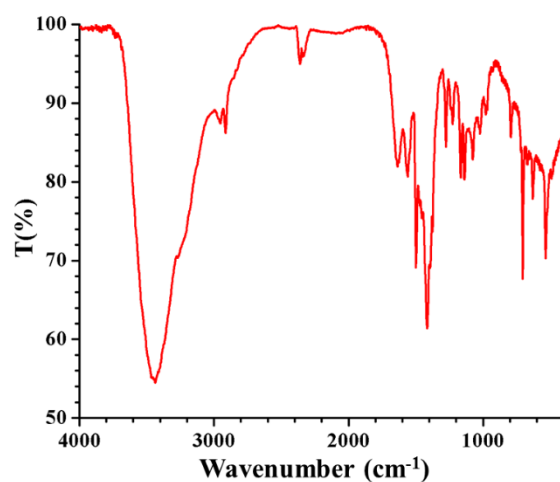
**Fig. S3** IR spectrum of the complex
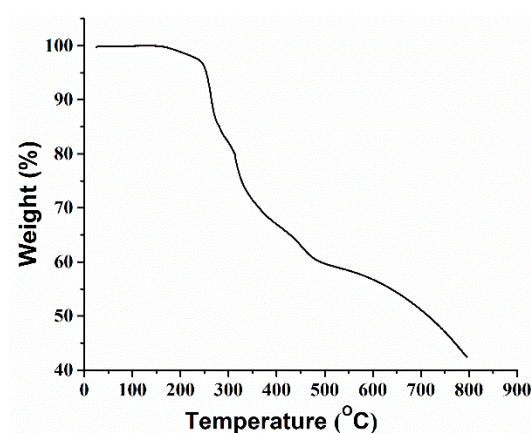


**Fig. S4** Thermogravimetric plot of the complex showing weight loss less than 2 % for $NH_3$ molecules (calculated 1.66 %) below 250 °C.
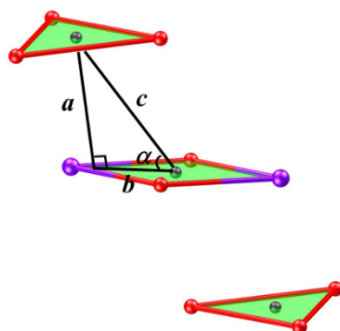


**Fig. S5** Schematic illustration of the inclined stacking modes showing planar distance *a* (2.773 Å), horizontal distance *b* (2.140 Å), centroid distance *c* (3.503 Å) and inclination angle $\alpha$ (52.34 °).
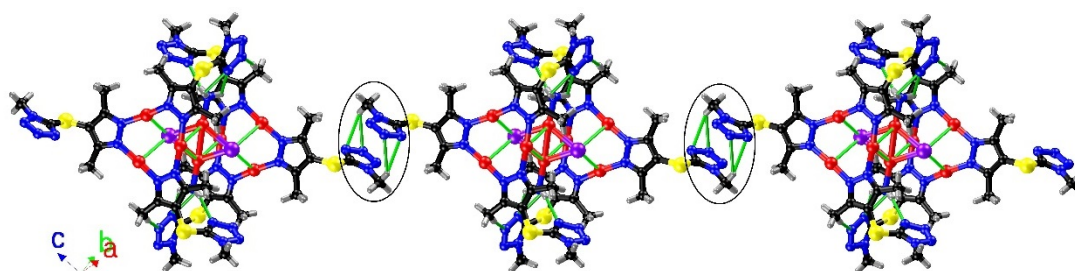
(a) N···H and π-π interactions (highlighted in cycle) through 1-methyl-tetrazole groups between these adducts. The centroid distances between tetrazole rings are about 3.4411(1) Å.
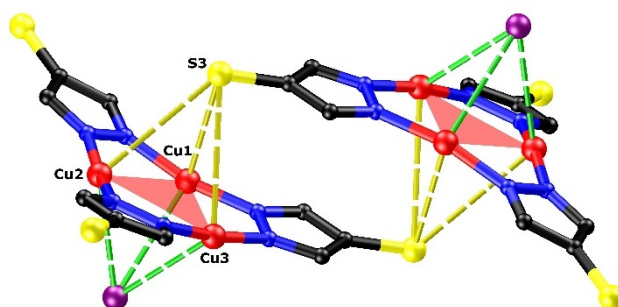


(b) Cu$_3$···S weak interactions showing Cu···S distances 3.58-3.94 Å, much larger than the sum of van der Waals radii of Cu and S atoms (1.40 + 1.80 = 3.20 Å).
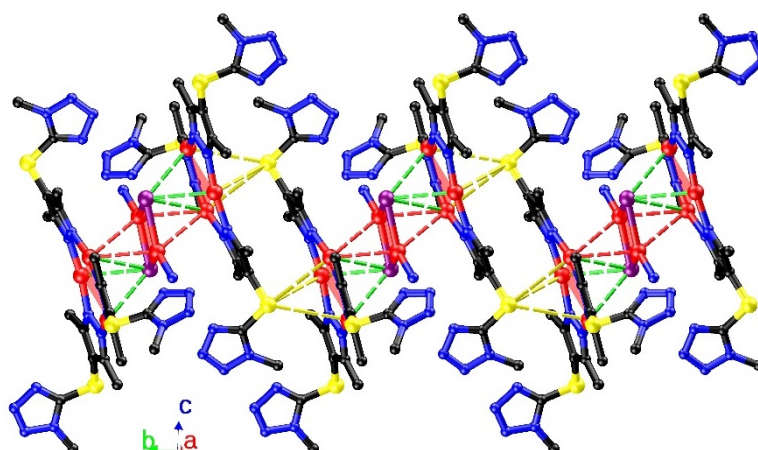


(c) Extended chains supported by Cu$_3$···S π acid-base interactions between the ternary adducts.

**Fig. S6** Weak interactions between the ternary adduct showing N···H, π-π (a), Cu$_3$···S (b c) interactions.

## Section 3: Hirshfeld Surface Analysis

**Hirshfeld Surface Calculations**. Hirshfeld surfaces,[S3] fingerprint plots were calculated using CrystalExplorer (version 3.1) software[S4] from the crystal structure coordinates supplied as CIF files (293 K). Hirshfeld surfaces with $d_{norm}$ (isovalue =

0.5) over the range −0.15 to 1.50 were mapped on $Cu_3L_3$ and $Cu_2I_2(NH_3)_2$ molecules. $d_{norm}$ is the function of distance defined as follow:

$$d_{norm} = \frac{d_i - r_i^{vdW}}{r_i^{vdW}} + \frac{d_e - r_e^{vdW}}{r_e^{vdW}}$$

where $d_i$ and $d_e$ refer to the distances from a point on the surface to the nearest nucleus inside and outside the surface, respectively, while $r_i^{vdW}$ and $r_e^{vdW}$ refer to the van der Waals radii of the atoms. The $d_{norm}$ surface map allows visualization of intermolecular interactions by displaying a surface with a red-white-blue color code. The red, white, as well as blue color regions in the surface mapped with $d_{norm}$ refer to the contact with the distance shorter than, equals to, and longer than sum of van der Waals radii, respectively. Each point on the Hirshfeld surfaces with $d_{norm}$ could be found on the corresponding 2D fingerprint with the coordinate of ($d_i$, $d_e$).
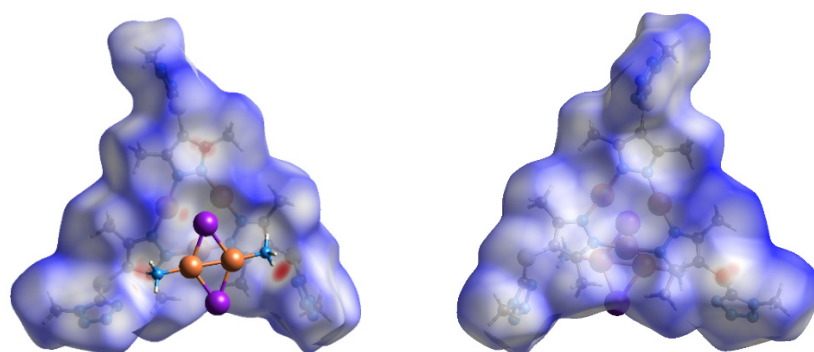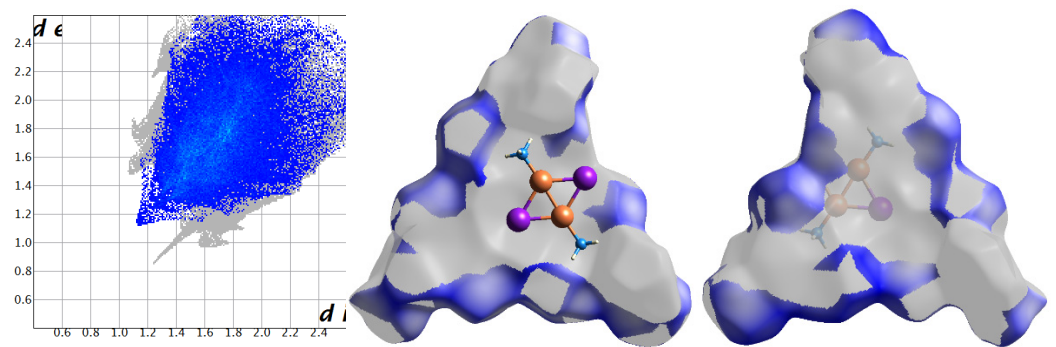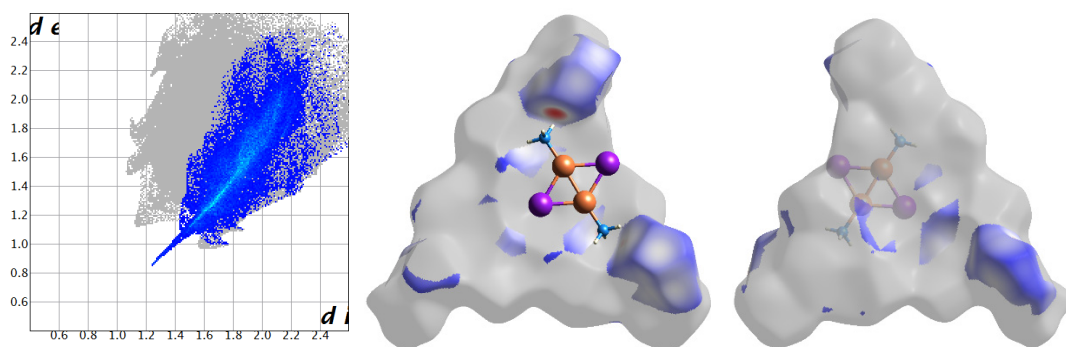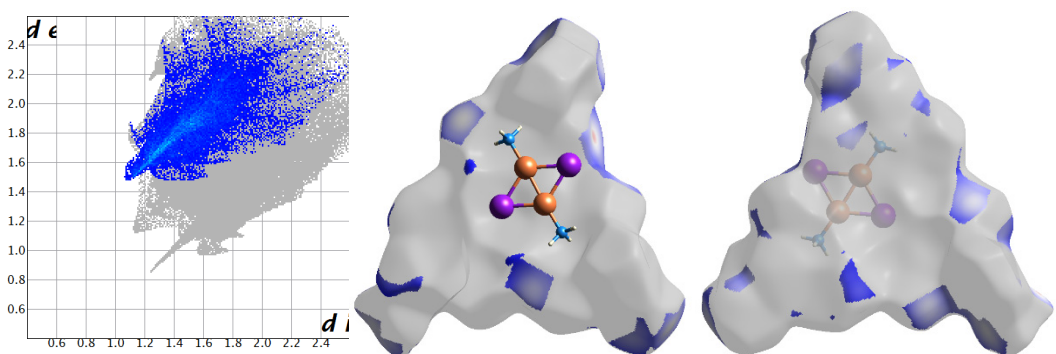


(a)
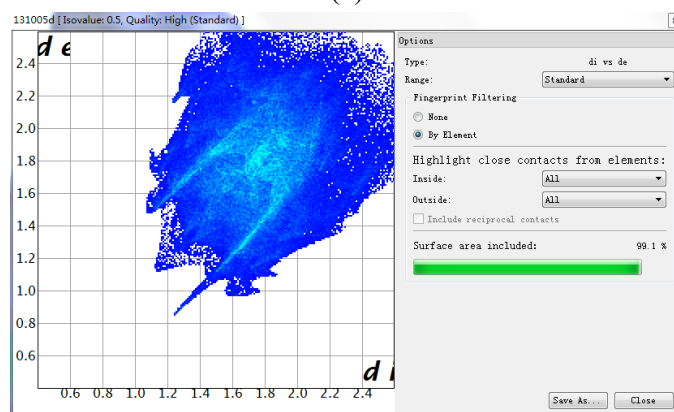


(b)

**Fig. S7** Hirshfeld surfaces mapped with $d_{norm}$ for $Cu_3L_3$ molecule showing close contact with one $Cu_2I_2(NH_3)_2$ molecule viewing from two sides (a) and the Fingerprint plot analysis results showing 99.1% contribution of close contact for the total surface (b).

(a) H-H 35.2%



(b) N-H 21.3%



(c) H-N 14.7%

**Fig. S8** Decomposed fingerprint plots (left) and Hirshfeld surfaces distribution (middle and right, $d_{norm}$ surface, highlight in color) displaying various intermolecular close contacts from one $Cu_3L_3$ molecule (inside) to other adjacent molecules (outside, $Cu_3L_3$ and $Cu_2I_2(NH_3)_2$) showing their percentage contributions to the Hirshfeld surface area. The full fingerprint and Hirshfeld surfaces appears beneath as a grey shadow.
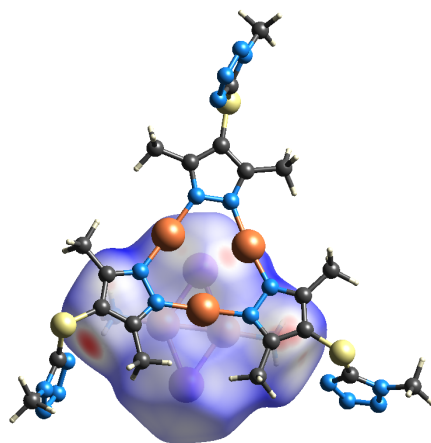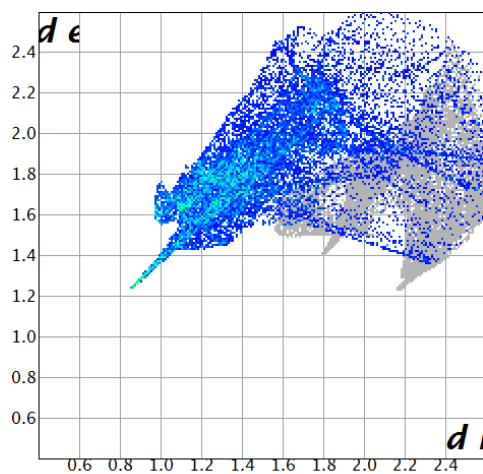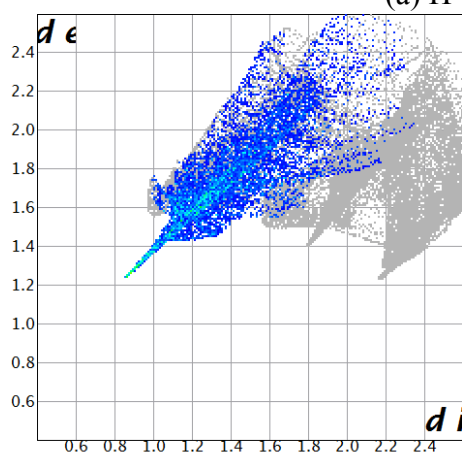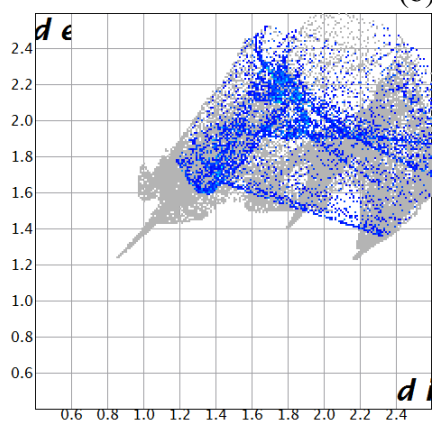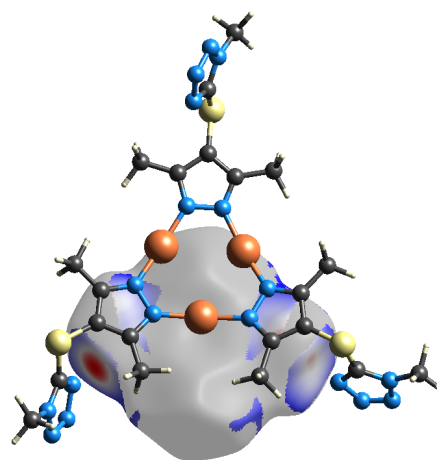
(a)
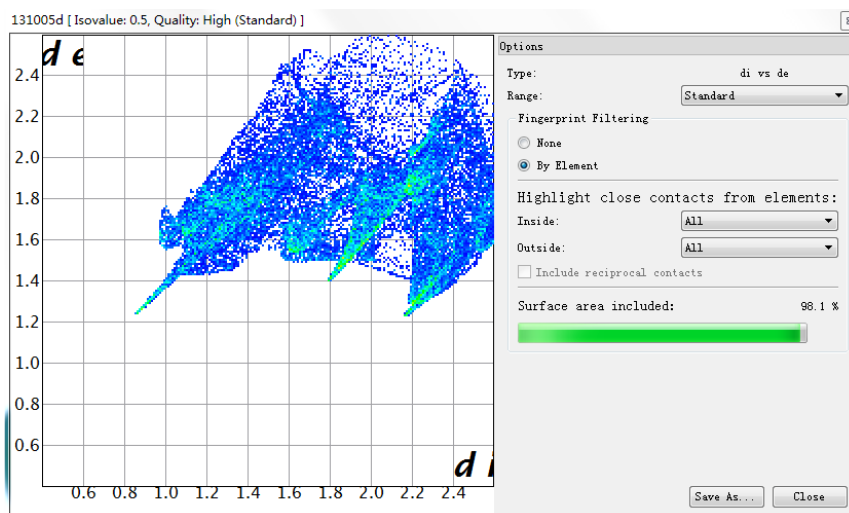


(b)

**Fig. S9** Hirshfeld surfaces ($d_{norm}$ surface) of $Cu_2I_2(NH_3)_2$ molecule showing close contact with one $Cu_3L_3$ molecule (a) and the Fingerprint plot analysis results showing 98.1% contribution of close contact for the total surface (b).
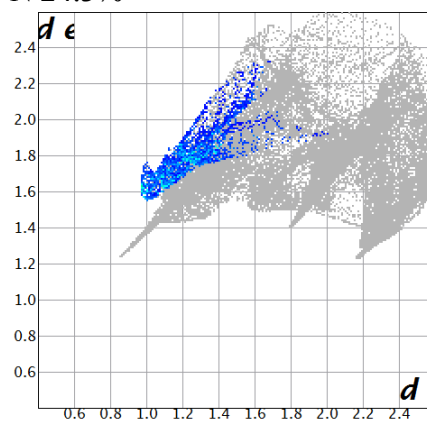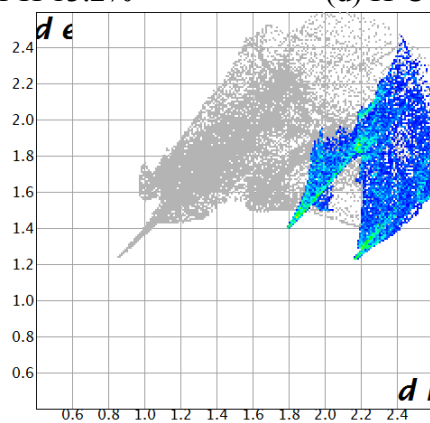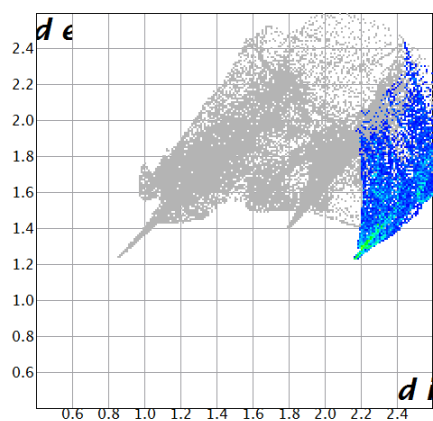
(a) H-all 47.3%



(b) H-N 24.3%



(c) H-H 13.2%    (d) H-C 8.6%



(e) I-all 39.5%

(f) I-H 19.3%
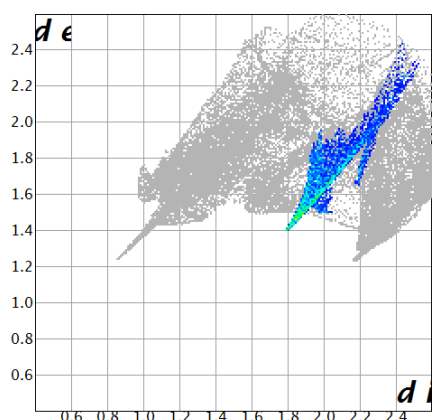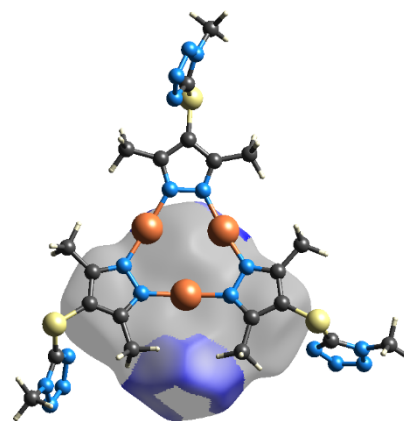


(g) I-Cu 12.5%



(h) Cu-Cu 5.2%

**Fig. S10** Decomposed fingerprint plots (left) displaying various intermolecular close contacts from one $Cu_2I_2(NH_3)_2$ molecule (inside) to other adjacent $Cu_3L_3$ molecules (outside) showing their percentage contributions to the Hirshfeld surface area. The full fingerprint and Hirshfeld surfaces appear beneath each decomposed plot as a grey shadow.

**Table S4** Various intermolecular close contacts and their percentage contribution to the Hirshfeld surface area from elements of one $Cu_3L_3$ molecule to other molecules.
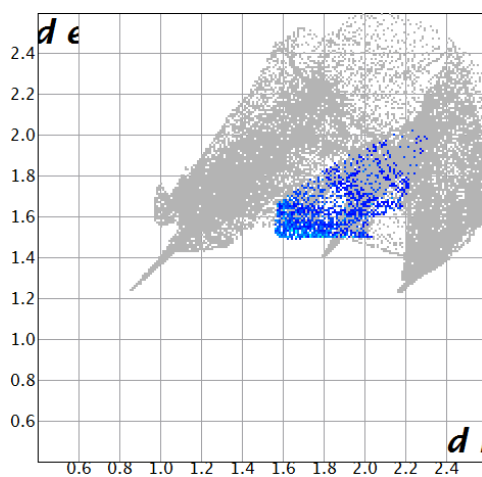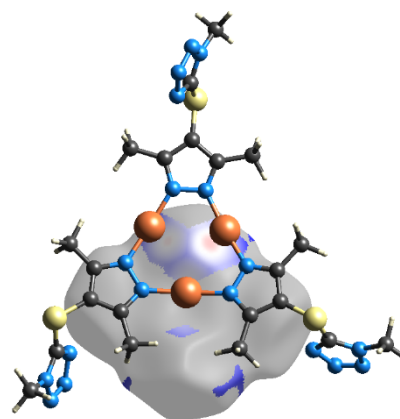
| $Cu_3L_3$ | Other molecules | Percentage Contribution (%) |
|---|---|---|
| all | H | 63.5 |
| | N | 19.1 |
| | I | 4.0 |
| N | all | 26.6 |
| | H | 21.3 |
| H | all | 56.4 |
| | N | 14.7 |
| | H | 35.2 |
| Cu | all | 5.0 |
| | I | 1.6 |
| | Cu | 0.7 |
| | S | 0.8 |
| | H | 1.9 |

**Table S5** Various intermolecular close contacts and their percentage contribution to the Hirshfeld surface area from elements of one $Cu_2I_2(NH_3)_2$ molecule to other molecules

| $Cu_2I_2(NH_3)_3$ | Other molecules | Percentage Contribution (%) |
|---|---|---|
| all | H | 33.6 |
| | N | 33.3 |
| | Cu | 18.9 |
| | C | 10.7 |
| H | all | 47.3 |
| | N | 24.3 |
| | H | 13.2 |
| | C | 8.6 |
| I | all | 39.5 |
| | Cu | 12.5 |
| | H | 19.3 |
| Cu | all | 11.2 |
| | Cu | 5.2 |

**Additional Descriptions for the Table S4 and Table S5:**

For $Cu_3L_3$ molecules, H···H (35.2 %), H···N (21.3%) and N···H (14.7%) contacts dominate its interactions with other $Cu_3L_3$ and $[Cu_2I_2(NH_3)_2]$, in which H···N (N···H) hydrogen interactions contribute 36.0 %. The shortest interactions, highlighted in black cycle in Fig. 2, is $H(NH_3)$···N(tetrazole) contacts (2.20799 Å), as stated above. For $[Cu_2I_2(NH_3)_2]$ molecules, the most contribution is H (47.3%) and I (39.5 %) atoms, in which the total of $H(NH_3)$···N(tetrazole) (24.3%), I···Cu (12.5%), I···H (19.3%) is 56.1%.

**Section 4: Diffuse Reflectance and Photoluminescence Properties**
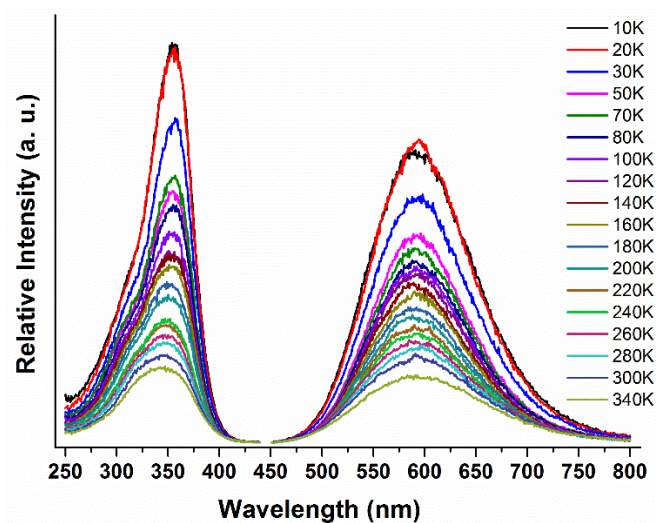


(a)
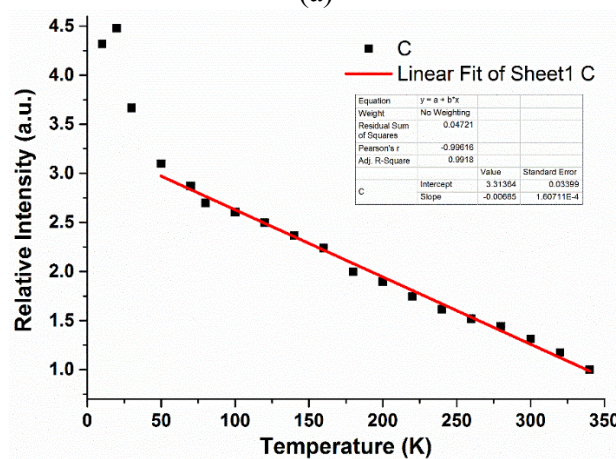


(b)

**Fig. S11** Excitation (monitored at 590 nm) and emission (excited at 345 nm) spectra from 10 K to 340 K (a) and linear fit plot of intensity-temperature showing good fitting result from 50 K to 340 K interval (b).
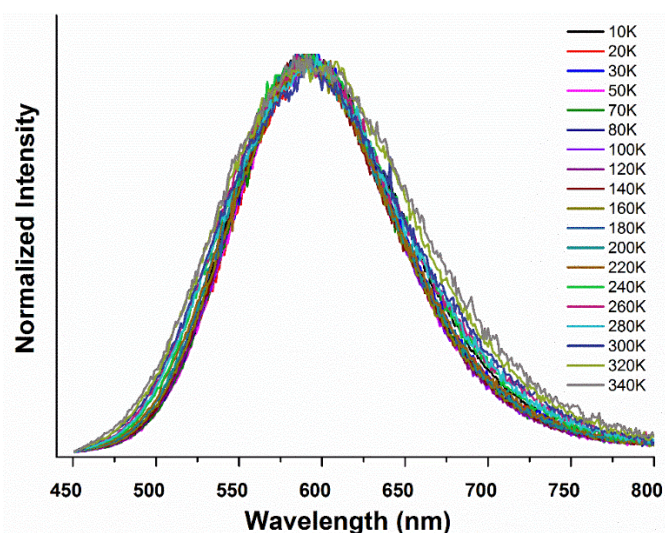
**Fig. S12** The normalized emission spectra showing no shifting of emission maxima and slightly increasing of full width at half maximum (FWHM) under higher temperature
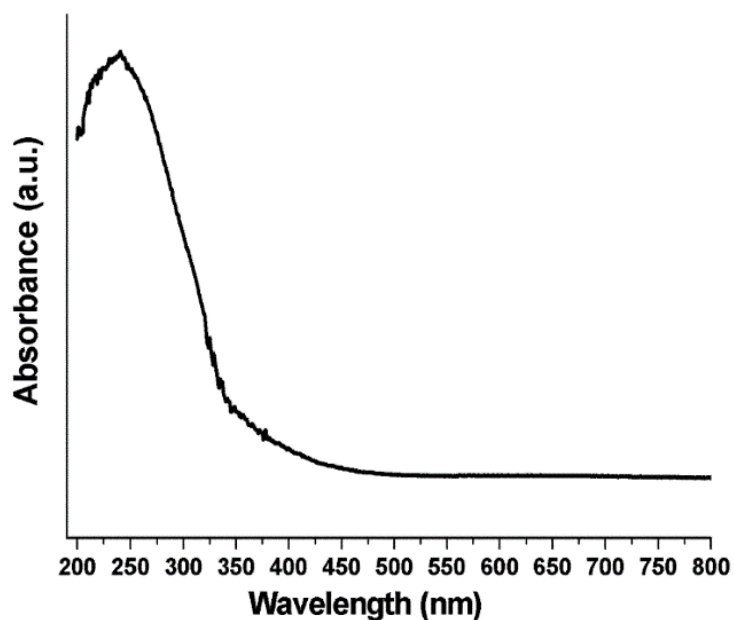


**Fig. S13** Diffuse reflectance solid-state UV-Vis spectrum of the complex.

**Table S6** Luminescence decay lifetimes ($\tau$, $\mu$s) and corresponding fractional contributions (%) of the solid-state sample from 10 K to 300 K monitored at 590 nm with excitation of 345 nm ($\chi^2$: fitting parameter).

| T (K) | 10 | 30 | 50 | 70 | 100 | 140 | 180 | 220 | 260 | 300 |
|---|---|---|---|---|---|---|---|---|---|---|
| $\tau_1$ (%) | 6.60 (79.31) | 6.43 (75.13) | 5.99 (62.12) | 6.33 (69.42) | 5.84 (61.59) | 5.30 (45.20) | 5.58 (58.94) | 5.01 (38.65) | 4.36 (31.57) | 5.16 (49.89) |
| $\tau_2$ (%) | 11.86 (20.69) | 11.07 (24.87) | 10.03 (37.88) | 10.32 (30.58) | 9.74 (38.41) | 9.00 (54.80) | 9.65 (41.06) | 8.66 (61.35) | 8.60 (68.43) | 9.50 (50.11) |
| $\chi^2$ | 1.294 | 1.140 | 1.155 | 1.261 | 1.131 | 1.086 | 1.141 | 1.544 | 1.362 | 1.092 |
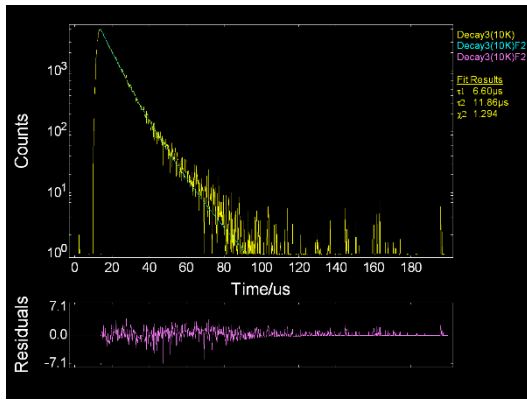
(a) 10 K
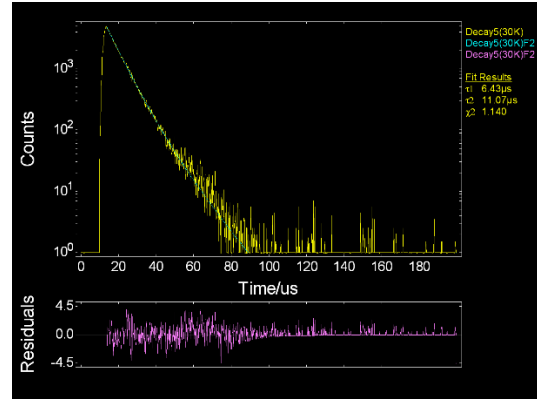
(b) 30 K
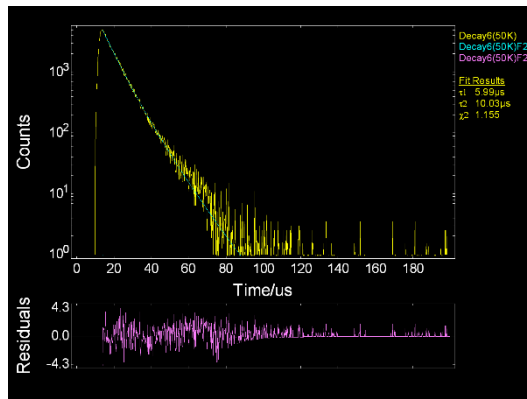
(c) 50 K
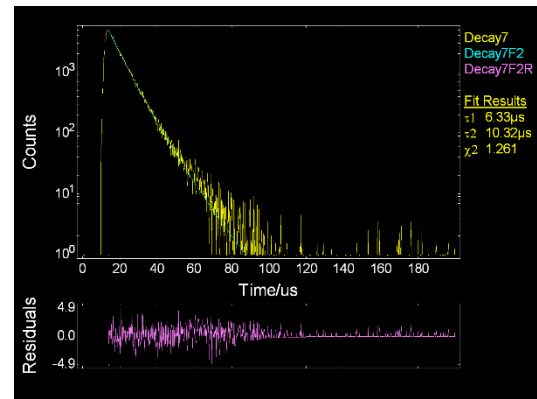
(d) 70 K
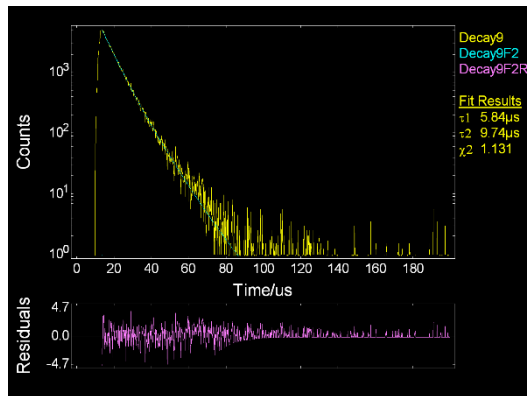
(e) 100 K
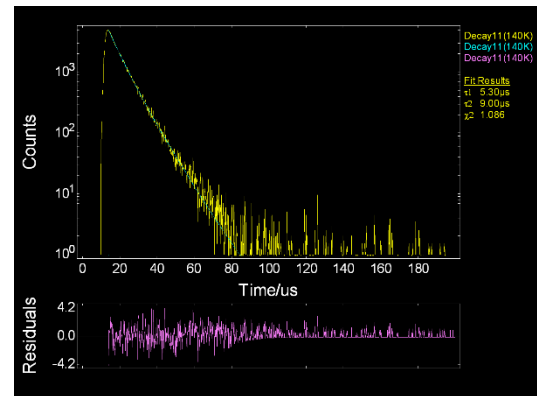
(f) 140 K
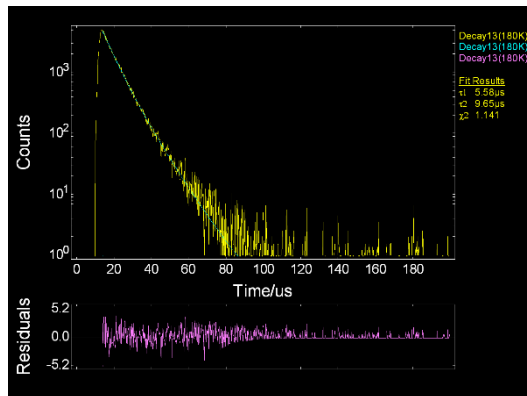
(g) 180 K
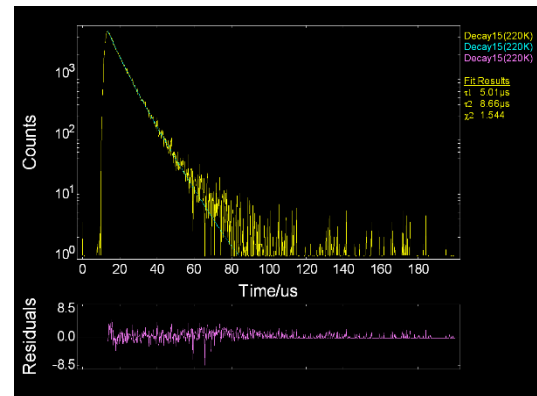
(h) 220 K
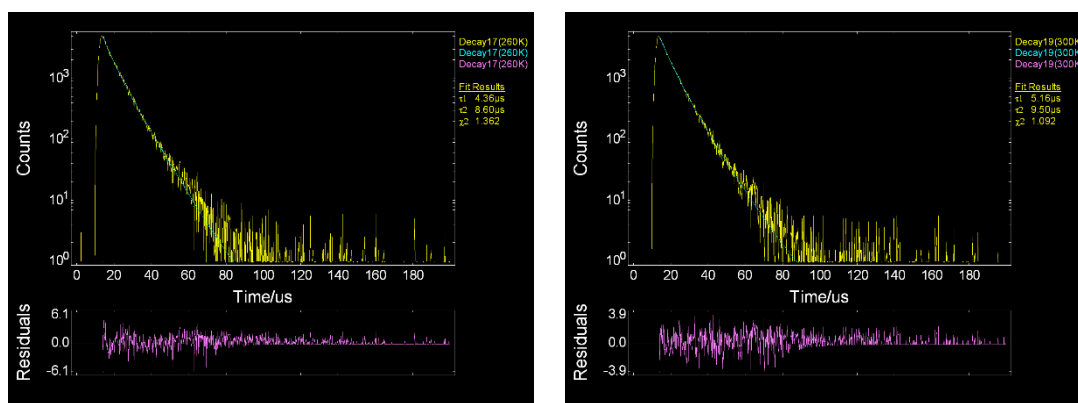
<div align="center">(i) 260 K            (j) 300 K</div>

**Fig. S14** Luminescence decay patterns of the complex monitored at corresponding excitation (345 nm) and emission (590 nm) in solid state under various temperatures (10~300 K).

## Section 5: Additional Theoretical Calculation Details

**Density Functional Theory (DFT) calculations**

The geometrical structures of the singlet ground states ($S_0$) and the lowest-lying triplet excited states ($T_1$) of the complex were optimized by using restricted (RDFT) and unrestricted DFT (UDFT) methods without consideration of symmetry constrains. All the calculations were carried out with Gaussian 09 software package [S5], and some of the output files were used as input files of Multiwfn software packages [S6] to perform wave function analysis. PBE0 functional [S7-S9] was used throughout, LANL2DZ basis set [S10] was used for Cu and I atoms while the 6-31G(d) basis set [S11] was employed for other atoms (C, N, S and H). Hirshfeld composition was analyzed by Multiwfn software packages.

**Time-Dependent Density Functional Theory (TDDFT) Calculations**

Based on the optimized geometries of $S_0$ and $T_1$ states, TDDFT method was used to calculate the phosphorescent spectra. Electron density difference (EDD) maps could be obtained to provide accurate assignments of excited states by calculating singlet-singlet spin-allowed and emission transition and then further treating the results by Multiwfn software packages [S12].

**Table S7** The calculated first 40 transitions based on the optimized $S_0$ state for the complex.

| No. | singlet-singlet spin-allowed transition | | | singlet-triplet spin-forbidden transition | |
|---|---|---|---|---|---|
| | E(eV) | λ(nm) | $f$ | E(eV) | λ(nm) |
| **1** | **3.930** | **315.5** | **0.0113** | 3.691 | **335.9** |
| 2 | 4.188 | 296.1 | 0.0000 | 3.972 | 312.2 |
| 3 | 4.236 | 292.7 | 0.0000 | 4.012 | 309.1 |
| 4 | 4.307 | 287.8 | 0.0074 | 4.062 | 305.2 |
| 5 | 4.426 | 280.2 | 0.0000 | 4.109 | 301.8 |
| 6 | 4.459 | 278.0 | 0.0001 | 4.110 | 301.7 |
| 7 | 4.464 | 277.8 | 0.0000 | 4.157 | 298.3 |
| 8 | 4.498 | 275.7 | 0.0033 | 4.221 | 293.8 |
| 9 | 4.498 | 275.6 | 0.0015 | 4.230 | 293.1 |
| **10** | **4.519** | **274.4** | **0.1631** | 4.273 | 290.1 |
| 11 | 4.562 | 271.8 | 0.0282 | 3.691 | 289.9 |
| 12 | 4.567 | 271.5 | 0.0000 | 3.972 | 289.3 |
| 13 | 4.657 | 266.2 | 0.0000 | 4.012 | 286.4 |
| 14 | 4.673 | 265.3 | 0.0748 | 4.062 | 285.2 |
| 15 | 4.713 | 263.1 | 0.0000 | 4.109 | 284.4 |
| 16 | 4.741 | 261.5 | 0.0314 | 4.110 | 281.3 |
| 17 | 4.745 | 261.3 | 0.0000 | 4.157 | 335.9 |
| 18 | 4.773 | 259.8 | 0.0000 | 4.221 | 312.2 |
| **19** | **4.778** | **259.5** | **0.1397** | 4.230 | 309.1 |
| 20 | 4.784 | 259.2 | 0.0000 | 4.273 | 305.2 |
| 21 | 4.798 | 258.4 | 0.0000 | 3.691 | 301.8 |
| 22 | 4.799 | 258.4 | 0.0303 | 3.972 | 301.7 |
| 23 | 4.828 | 256.8 | 0.0495 | 4.012 | 298.3 |
| 24 | 4.853 | 255.5 | 0.0000 | 4.062 | 293.8 |
| 25 | 4.864 | 254.9 | 0.0354 | 4.109 | 293.1 |
| 26 | 4.869 | 254.7 | 0.0407 | 4.110 | 290.1 |
| 27 | 4.874 | 254.4 | 0.0000 | 4.157 | 289.9 |
| 28 | 4.899 | 253.1 | 0.0064 | 4.221 | 289.3 |
| 29 | 4.920 | 252.0 | 0.0000 | 4.230 | 286.4 |
| 30 | 4.926 | 251.7 | 0.0000 | 4.273 | 285.2 |
| 31 | 4.932 | 251.4 | 0.0249 | 3.691 | 284.4 |
| 32 | 4.938 | 251.1 | 0.0241 | 3.972 | 281.3 |
| 33 | 4.942 | 250.9 | 0.0009 | 4.012 | 335.9 |
| 34 | 4.943 | 250.8 | 0.0486 | 4.062 | 312.2 |
| 35 | 4.947 | 250.6 | 0.0000 | 4.109 | 309.1 |
| 36 | 4.953 | 250.3 | 0.0183 | 4.110 | 305.2 |
| 37 | 4.962 | 249.9 | 0.0258 | 4.157 | 301.8 |
| 38 | 4.966 | 249.7 | 0.0000 | 4.221 | 301.7 |
| 39 | 4.979 | 249.0 | 0.0000 | 4.230 | 298.3 |
| 40 | 4.992 | 248.4 | 0.0131 | 4.273 | 293.8 |

**Table S8** The calculated absorption spectra, the electron density difference (EDD) maps and the orbital transitions of the selected vertical singlet excited states for the complex (isovalue = 0.0004 a.u.).
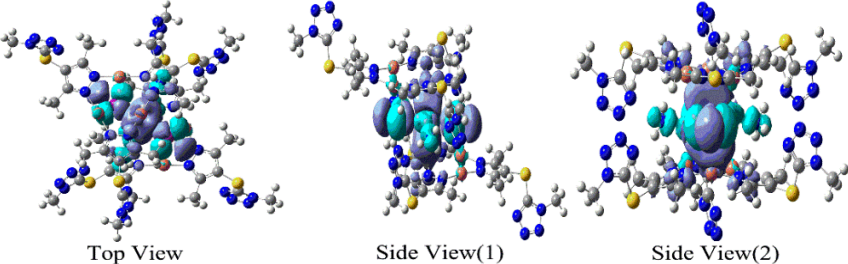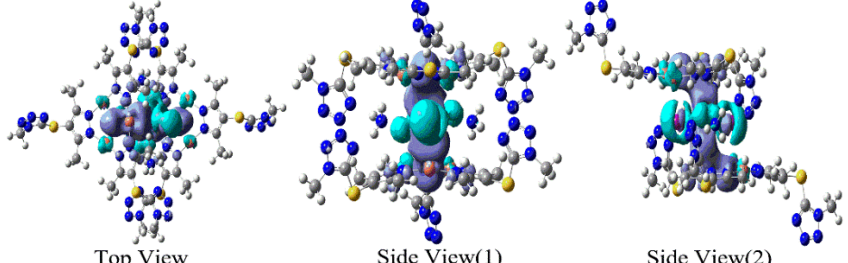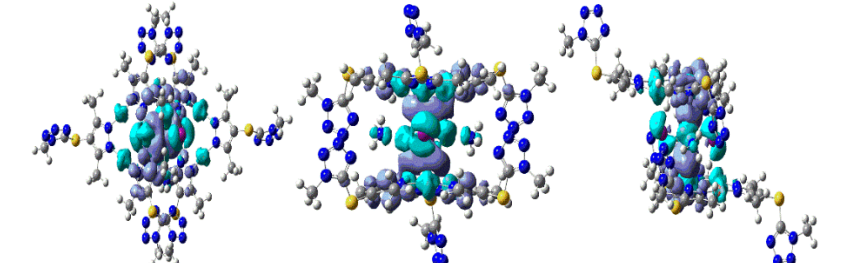
| No. | E(eV) | λ(nm) | $f$ | EDD | Major transitions and contributions (H = HOMO, L = LUMO) | Type |
|---|---|---|---|---|---|---|
| 1 | 3.930 | 315.5 | 0.0113 | Top View  Side View(1)  Side View(2) | H→L+5 (84%) | [1]CC, [1]XLCT, [1]LLCT |
| 10 | 4.519 | 274.4 | 0.1631 | Top View  Side View(1)  Side View(2) | H-2→L+5 (56%) H-1→L+4 (13%) | [1]CC, [1]XLCT, [1]LLCT |
| 19 | 4.778 | 259.5 | 0.1397 | Top View  Side View(1)  Side View(2) | H-12→L+5 (7%) H-6→L+7 (8%) H-1→L+7 (40%) | [1]CC, [1]XLCT, [1]LLCT |

**Table S9** The Hirshfeld compositions (%) of selected MOs in the ground state at the PBE0 level of theory for the complex.

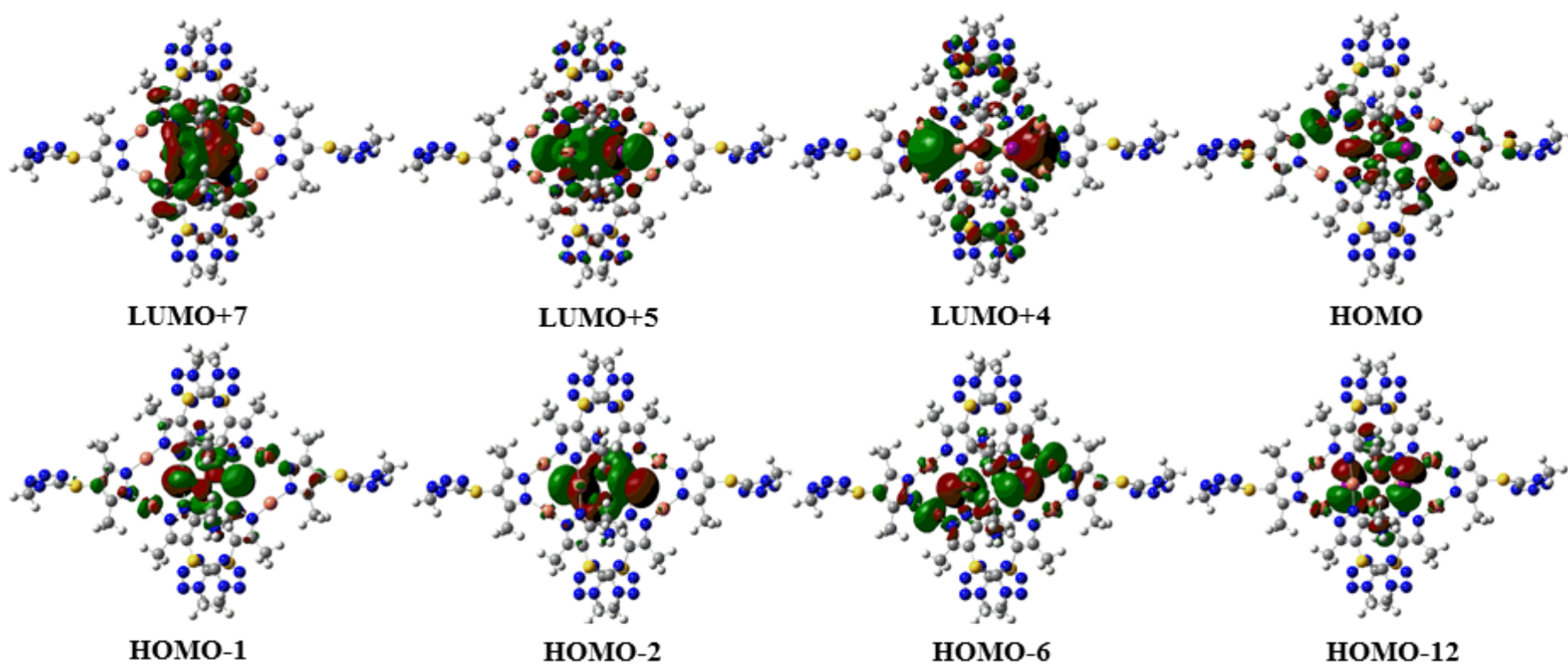| Fragment | HOMO-12 | HOMO-6 | HOMO-2 | HOMO-1 | HOMO | LUMO | LUMO+4 | LUMO+5 | LUMO+7 |
|---|---|---|---|---|---|---|---|---|---|
| Cu from $Cu_3L_3$ | 52.64 | 26.58 | 5.39 | **40.14** | 8.58 | 2.73 | 49.50 | **17.63** | **18.73** |
| Cu from $Cu_2I_2(NH_3)_2$ | 19.86 | 37.72 | **52.48** | **20.30** | **46.73** | 0.08 | 0.74 | **17.49** | 8.93 |
| I | 1.01 | 16.27 | **35.98** | **20.92** | **31.67** | 0.26 | 4.41 | 5.34 | 6.27 |
| L | 25.83 | 15.95 | 4.32 | **15.93** | 4.86 | 96.81 | 45.24 | **57.75** | **65.14** |
| $NH_3$ | 0.66 | 3.48 | 1.83 | 2.71 | 8.16 | 0.12 | 0.11 | 1.79 | 0.93 |

**Fig. S15** Selected molecular orbitals (MOs) at the PBE0 level of theory for the complex (isovalue = 0.02).
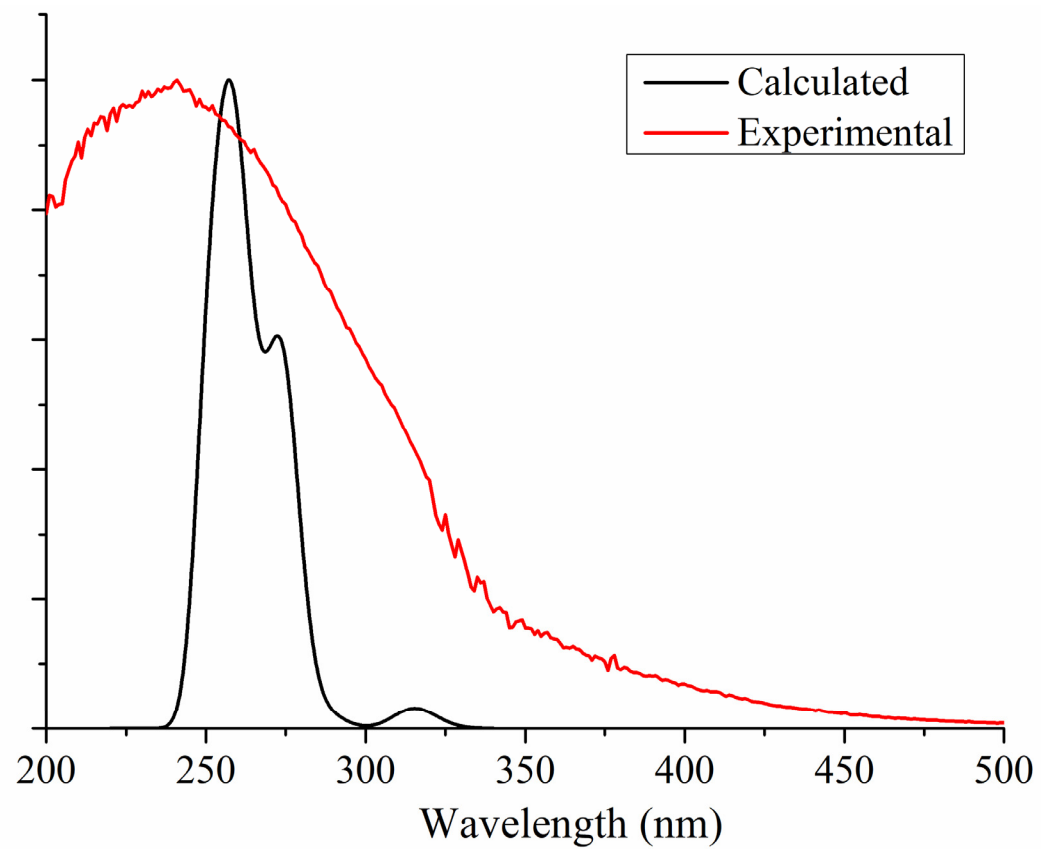
**Fig. S16** Comparison of normalized calculated absorption spectrum (black) and experimental UV-Vis diffuse reflectance spectrum (red) in solid state.
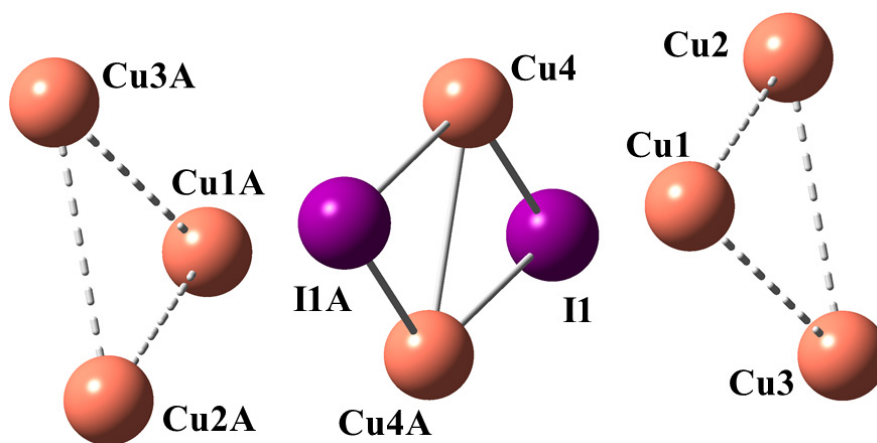
(a) The optimized structure of S$_0$ state
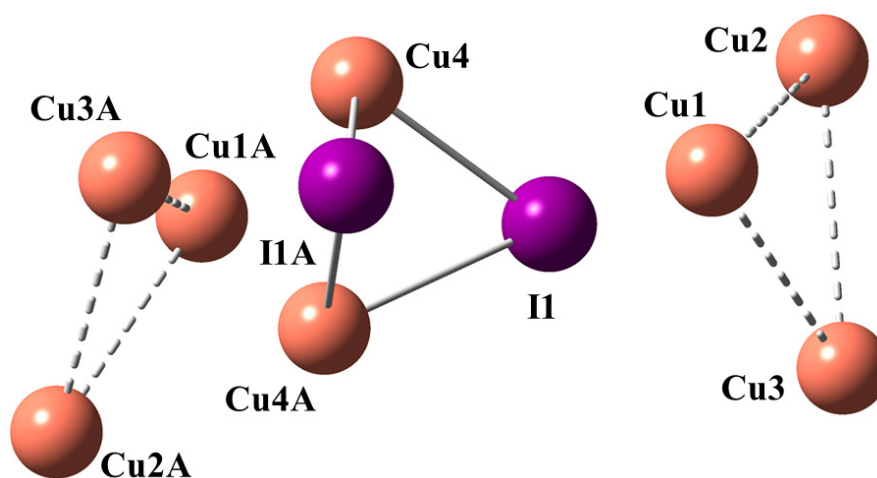


(b) The optimized structure of T$_1$ state

**Fig. S17** The optimized Cu$_3$···Cu$_2$I$_2$···Cu$_3$ structural geometries for S$_0$ state (a) and T$_1$ state (b), showing severely distorted geometry of T$_1$ state compared with S$_0$ state. Note that the labels are consistent with crystal structure descripted in Fig. 1, but the label symbol "A" does not mean any symmetrical relations because symmetry constrains were not taken into considerations for theoretical calculation.

**Table S10** The selected bond lengths (Å) and bond angles (°) of optimized $S_0$ and $T_1$ geometrical structures for complex at the PBE0/(LANL2DZ+6-31G(d)) level of theory, together with the experimental value (The data in brackets are the deviation percentage (%) from the experimental values (293 K)).

| Parameters | Complex | | |
|:---:|:---:|:---:|:---:|
| | $S_0$ | $T_1$ | Exp |
| Cu1−Cu2 | 3.221 | 3.230 | 3.120 |
| Cu2−Cu3 | 3.208 | 3.222 | 3.172 |
| Cu3−Cu1 | 3.238 | 3.242 | 3.241 |
| Cu4−Cu4A | 2.688 (+12.84) | 2.531 (+6.25) | 2.382 |
| Cu1A−Cu2A | 3.221 | 2.879 (-7.72) | 3.120 |
| Cu2A−Cu3A | 3.208 | 2.981 (-6.02) | 3.172 |
| Cu3A−Cu1A | 3.238 | 3.036 (-6.33) | 3.241 |
| Cu1−I1 | 3.475 | 3.469 | 3.476 |
| Cu2−I1 | 3.155 | 3.460 (+8.22) | 3.197 |
| Cu3−I1 | 3.412 | 3.264 | 3.303 |
| Cu4−I1 | 2.655 | 2.874 (+13.42) | 2.534 |
| Cu4−I1A | 2.754 | 2.880 (+11.76) | 2.577 |
| Cu4A−I1 | 2.754 | 3.469 (+34.61) | 2.577 |
| Cu4A−I1A | 2.655 | 2.811 (+10.93) | 2.534 |
| Cu1A−I1A | 3.476 | 4.911 (+41.28) | 3.476 |
| Cu2A−I1A | 3.155 | 2.983 (-6.69) | 3.197 |
| Cu3A−I1A | 3.411 | 5.049 (+52.81) | 3.304 |
| Cu1−Cu4 | 2.789 (-9.59) | 2.941 | 3.085 |
| Cu1−Cu4A | 3.343 | 4.151 (+31.15) | 3.165 |
| Cu1A−Cu4 | 3.343 | 2.779 (-12.20) | 3.165 |
| Cu1A−Cu4A | 2.789 (-9.59) | 4.599 (+49.08) | 3.085 |
| Cu2−I1−Cu3 | 58.3 | 57.2 | 58.4 |
| Cu4−I1−Cu4A | 59.6 | 53.7 | 55.5 |
| Cu4−I1A−Cu4A | 59.6 | 52.8 | 55.5 |
| Cu2A−I1A−Cu3A | 58.3 | 32.1 | 58.4 |
| Cu1−Cu2−Cu3 | 60.0 | 60.0 | 58.2 |
| Cu1A−Cu2A−Cu3A | 60.0 | 57.2 | 58.2 |
| Cu4−I1−Cu4A−I1A | 0.0 | 50.8 | 0.0 |
| I1−Cu4−Cu4A−I1A | 180.0 | 119.9 | 180.0 |

**Table S11** The calculated phosphorescent emission, the electron density difference (EDD) maps and the orbital transition for complex at the TD-PBE0 level of theory (isovalue = 0.0004 a.u.).
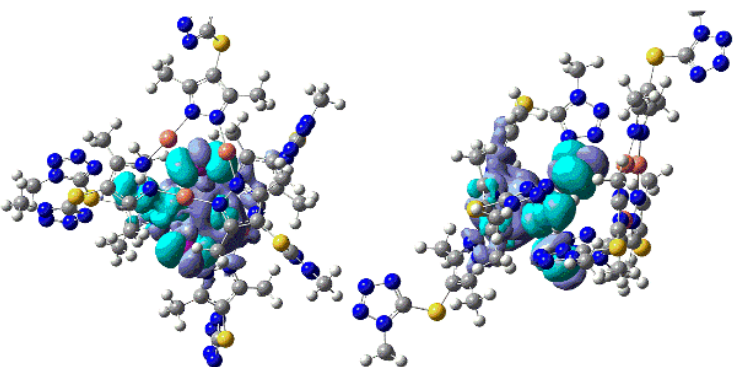
| E(eV) | λ(nm) | EDD | Major transitions and contributions | Type |
|-------|-------|-----|-------------------------------------|------|
| 1.524 | 813.6 | Top View     Side View | HSOMO→LSOMO (89%) | $^3$CC, $^3$XLCT, $^3$MLCT |

**Table S12** The Hirshfeld compositions (%) of selected MOs in the $T_1$ state at the PBE0 level of theory for complex.

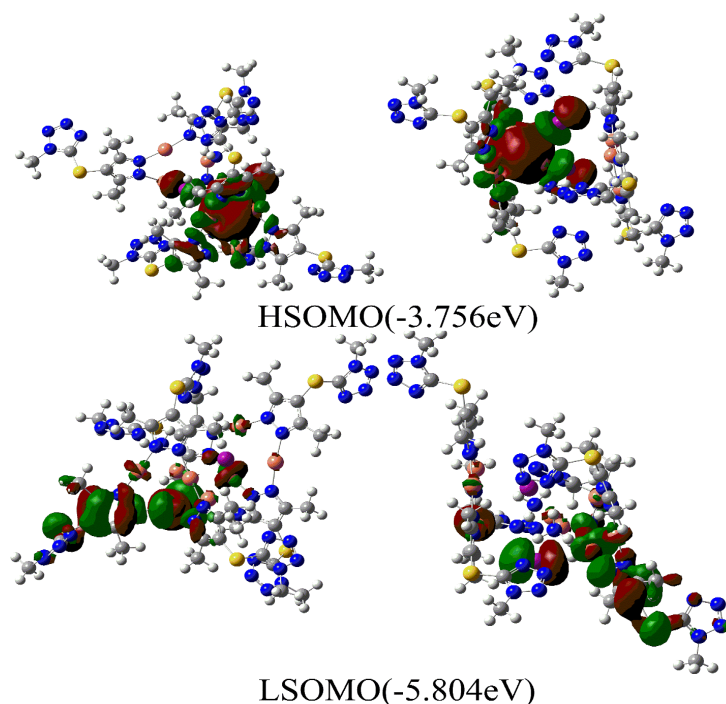| Fragment | LSOMO | HSOMO |
|----------|-------|-------|
| Cu from $Cu_3L_3$ | 41.90 | 39.86 |
| Cu from $Cu_2I_2$ | 1.51 | 23.20 |
| I | 17.76 | 17.15 |
| L | 38.69 | 18.27 |
| $NH_3$ | 0.14 | 1.52 |

HSOMO(-3.756eV)

LSOMO(-5.804eV)

**Fig. S18** Spatial plots of the selected molecular orbitals of the $T_1$ state optimized geometry at the PBE0 level of theory for the complex (isovalue = 0.02)
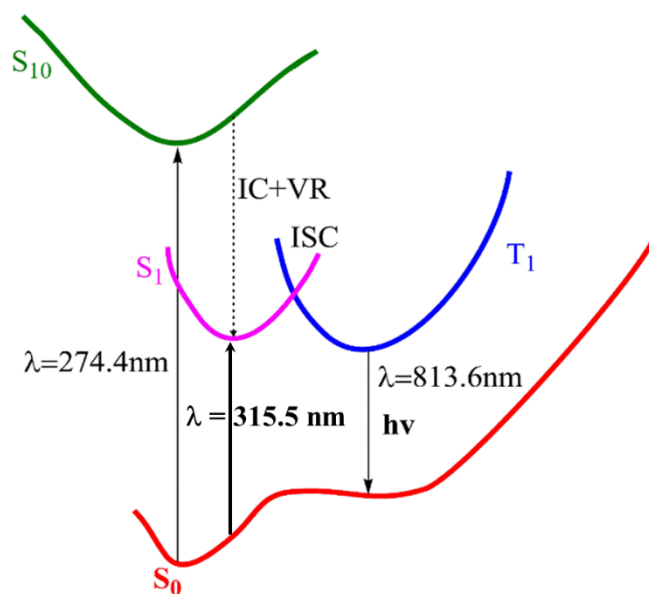


**Fig. S19** Simplified Jablonski diagram depicting the photophysical processes of the vertical $S_0 \rightarrow S_{10}$ and $S_0 \rightarrow S_1$ excitation, the internal conversion (IC) and intersystem crossing (ISC), and $T_1 \rightarrow S_0$ emission decay.

# References

S1 (a) Z. Yoshida, H. Ogoshi, T. Tokumitsu, *Tetrahedron*, 1970, **246**, 2987. (b) B. S. Zheng, X.-Y. Zhang, H.-W. Zhu, S.-X. Luo, L. F. Lindoy, J. C. McMurtrie, P. Turner, G. Wei, *Dalton Trans.*, 2005, 1349. (c) T.-J. Won, J. K. Clegg, L. F. Lindoy, J. C. McMurtrie, *Cryst. Growth Des.,* 2007, **7**, 972.

S2 G. M. Sheldrick, *Acta Crystallogr. A* 2008, **64**, 112.

S3 M. A. Spackman, D. Jayatilaka, *CrystEngComm* 2009, **11**, 19.

S4 S. K. Wolff, D. J. Grimwood, J. J. McKinnon, M. J. Turner, D. Jayatilaka, M. A. Spackman, CrystalExplorer, version 3.1; University of Western Australia: Crawley, Australia, 2012.

S5 M. J. Frisch, G. W. Trucks, H. B. Schlegel, G. E. Scuseria, M. A. Robb, J. R. Cheeseman, G. Scalmani, V. Barone, B. Mennucci, G. A. Petersson, H. Nakatsuji, M. Caricato, X. Li, H. P. Hratchian, A. F. Izmaylov, J. Bloino, G. Zheng, J. L. Sonnenberg, M. Hada, M. Ehara, K. Toyota, R. Fukuda, J. Hasegawa, M. Ishida, T. Nakajima, Y. Honda, O. Kitao, H. Nakai, T. Vreven, Jr. J. A. Montgomery, J. E. Peralta, F. Ogliaro, M. Bearpark, J. J. Heyd, E. Brothers, K. N. Kudin, V. N. Staroverov, R. Kobayashi, J. Normand, K. Raghavachari, A. Rendell, J. C. Burant, S. S. Iyengar, J. Tomasi, M. Cossi, N. Rega, J. M. Millam, M. Klene, J. E. Knox, J.B. Cross, V. Bakken, C. Adamo, J. Jaramillo, R. Gomperts, R. E. Stratmann, O. Yazyev, A. J. Austin, R. Cammi, C. Pomelli, J. Ochterski, R. L. Martin, K. Morokuma, V. G. Zakrzewski, G. A. Voth, P. Salvador, J. J. Dannenberg, S. Dapprich, A. D. Daniels, O. Farkas, J. B. Foresman, J. V. Ortiz, J. Cioslowski, D. J. Fox, GAUSSIAN 09 (Revision A.02), Gaussian, Inc., Wallingford, CT, 2009.

S6 T. Lu, F. W. J. Chen, *Comp. Chem.* 2012, **33**, 580.

S7 J. P. Perdew, K. Burke, M. Ernzerhof, *Phys. Rev. Lett.* 1996, **77**, 3865.

S8 J. P. Perdew, K. Burke, M. Ernzerhof, *Phys. Rev. Lett.* 1997, **78**, 1396.

S9 C. Adamo, V. Barone, *Theor. Chem. Acc.* 2000, **105(2)**, 169.

S10 P. J. Hay, W. R. Wadt, *J. Chem. Phys.* 1985, **82**, 270.

S11 J. E. Del Bene, *Chem. Phys. Lett.* 1983, **94(2)**, 213.

S12 Multiwfn manual, version 3.3.8, http://multiwfn.codeplex.com/.